



OPEN

# Mode Conversion of Propagating Surface Plasmons in Nanophotonic Networks Induced by Structural Symmetry Breaking

SUBJECT AREAS:  
NANOPHOTONICS AND  
PLASMONICS  
NANOSCIENCE AND  
TECHNOLOGY

Received  
13 March 2014

Accepted  
28 April 2014

Published  
16 May 2014

Correspondence and  
requests for materials  
should be addressed to  
H.W. (weihong@iphy.  
ac.cn) or H.X.X.  
(hxxu@iphy.ac.cn)

Deng Pan, Hong Wei, Zhili Jia & Hongxing Xu

Institute of Physics, Chinese Academy of Sciences and Beijing National Laboratory for Condensed Matter Physics, Beijing 100190, China.

Nanophotonic plasmon circuits may play important roles in next-generation information technology as semiconductor-based electronics is approaching the physical limit. The functions of such circuits rely on the rigorous control of plasmon propagation. One important aspect of such control is controlling the conversion of different plasmon modes for designed plasmon routing in complex nanophotonic networks. Here, for the first time, we experimentally prove that the conversion of plasmon modes occurs widely in metallic nanowire waveguides, the basic components of plasmonic circuits, by introducing local structural symmetry breaking. In further simulations for the structure of a nanowire with a particle in its proximity, it is shown that the mode conversions originate from the redistribution of electric field on the wave front which is caused by the scattering of localized modes in the nanogap and on the nanoparticle. This mode conversion effect can be applied to flexibly control the plasmon propagation behavior in plasmonic nanowire networks.

Plasmonics is a booming research field addressing topics related to surface plasmons, including enhanced light-matter interaction<sup>1–4</sup>, subdiffraction imaging<sup>5,6</sup>, integrated photonic circuits<sup>7–9</sup> and so on. Confronted with the physical limit that the semiconductor-based electronics is approaching, plasmonic circuits are promising for the future information technology as they keep the photons' advantages of high speed and wide bandwidth but avoid the dimension restriction caused by diffraction limit of light. Noble metallic nanowire (NW) supporting propagating surface plasmon polaritons (SPPs), have shown large application potentials in the plasmonic circuits. These wires can be used not only for basic nanophotonic devices such as waveguides<sup>10,11</sup>, resonators<sup>12,13</sup> and nanoantennas<sup>14,15</sup>, but also for quantum information researches<sup>16–19</sup>. Especially, the NW-based network can work as optical routers<sup>20,21</sup> and logic gates<sup>22,23</sup>. The routing and logic functions in the NW-based network rely on suitable SPP propagation manners in the NW, such as zigzag<sup>22,23</sup> and chiral<sup>24</sup> propagation, resulting from the superpositions of different SPP modes with proper phase relations. Therefore, controlling the excitation and conversion of different SPP modes is the basis for controlling SPP propagation in the NW network to realize advanced functions.

The steering of localized plasmon modes in metallic nanostructures can be achieved by structural symmetry breaking which lifts the degeneracy of the system and leads to the interaction between the orthogonal modes. For example, by introducing structural symmetry breaking, coupling between the bright dipole mode and dark mode occurs, thereby making it possible to excite the dark mode<sup>25,26</sup>. This coupling results in the Fano resonance<sup>27,28</sup> and plasmon-induced transparency<sup>29,30</sup>. Symmetry-broken nanoantennas can concentrate the modes of different frequencies at selected positions<sup>31</sup>, and mediate the radiation in the far field in various directions<sup>32</sup>. Symmetry-broken metallic split ring resonators<sup>33,34</sup> can show a magnetic response and negative effective permeability at certain frequency by tuning the resonant modes, which can be applied for negative refraction and superlensing. It is expected that the structural symmetry breaking can also induce the interaction between modes of the propagating plasmons and provide an efficient method for controlling SPP propagation.

In the present work, we show experimentally that the conversion of SPP modes occurs widely in structural-symmetry-broken NWs. These direct and tunable conversions of different modes on the NW are highly desired for adjusting the mode proportion and giving flexible control on SPP propagation. The conversion is shown to



originate from the symmetry change of wave front induced by the structural symmetry breaking. A model system composed of a silver NW and a silver nanoparticle is investigated carefully in simulations. The physical picture of the conversion is shown as the field redistribution on the wave front which results from scattering of the localized modes in the nanogap and on the nanoparticle. This mode conversion mechanism provides a versatile approach for controlling SPP propagation at the nanoscale, which is demonstrated in a structure to be used as a switch.

## Results

In experiments, chemically synthesized Ag NWs and nanoparticles were deposited on a glass substrate. Three typical kinds of NW-based

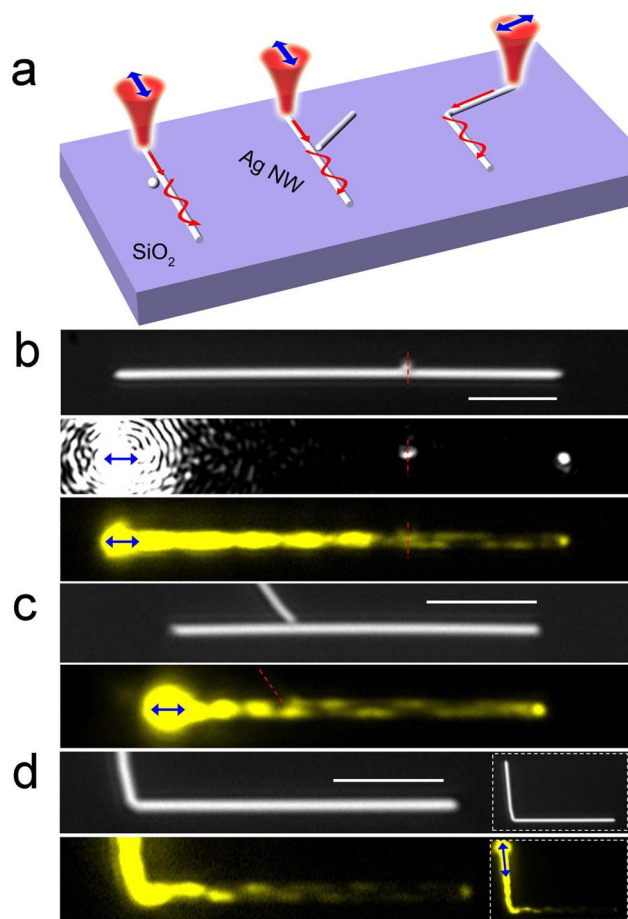


**Figure 1 | Experimental observation of mode conversion in NWs induced by structural symmetry breaking.** (a) Schematic illustration for three kinds of symmetry-broken NW-based structures. Laser light of 633 nm wavelength is focused on the ends of the NWs to excite the SPPs, with parallel polarizations (indicated by blue arrows). (b) A NW with a nanoparticle placed nearby. Top: white light optical image of the nanoparticle-NW structure. Middle: scattering image. Bottom: QD fluorescence image. (c–d) Branched NW and bent NW. Top: white light optical images. Bottom: QD fluorescence images. The red dashed lines in (b) and (c) are guides for eye to show the position of the introduced structures. The insets in (d) show the intact images of the bent wire. The double head blue arrows indicate the polarization of the excitation light. The scale bars in (b), (c) and (d) are 5  $\mu\text{m}$ . The radius of the NWs is about 150 nm. The  $\text{Al}_2\text{O}_3$  thickness is 50 nm for the structure in (b), and 30 nm for the structures in (c) and (d) (see Figs. S1 and S2 in supplementary information for nanoparticle-NW structures with  $\text{Al}_2\text{O}_3$  layer of 30 nm thickness). In all the QD emission images, the symmetric field distributions become zigzag shapes after the symmetry-broken regions.

structures can be found in the sample, including particle-NW structure, branched NW and bent NW as schematically shown in Fig. 1(a). The branched NW here is occasionally formed, which can also be constructed by micro-manipulation method<sup>22,23</sup>. Then they were coated with a 30 nm or 50 nm thick  $\text{Al}_2\text{O}_3$  layer to separate the subsequently deposited CdSe/ZnS core/shell quantum dots (QDs) with central emission wavelength of about 655 nm. The propagating SPP waves on the NW were launched by focusing a laser beam at one end of the NW through an objective, with the polarization of the laser light parallel to the NW. The fluorescence of QDs can reveal the local electric field distributions of the SPPs on the NWs.

The experimental results for the mode conversion in the three structures are shown in Figs. 1(b)–(d). The top panel of Fig. 1(b) shows the optical image of a particle-NW structure. After excitation by direct illumination on the NW end, the SPPs propagating on the NW were partly scattered by the particle, showing visible scattering light, and the remaining power propagates to the other end, as shown in the middle panel of Fig. 1(b). As can be seen from the QD fluorescence image [bottom panel in Fig. 1(b)], the excited SPPs first showed a symmetric field distribution, resulting from the symmetry of the forefront of the system. The symmetry of the structure was broken near the particle, which in turn influenced the symmetry of the propagating SPP field. After interaction with the particle, the field turned into a zigzag shape (more experimental results for particle-NW structure are shown in supplementary information). Local structural symmetry breaking can also be realized by introducing another NW or bending the NW, as shown in Figs. 1(c) and 1(d). Mode conversions also occurred in these samples as demonstrated by the changes of the near field distributions from symmetric patterns to zigzag.

Simulations using finite-difference time-domain (FDTD) method were performed for the three experimental structures and the results are shown in Fig. 2. The structures in our simulation model used the same parameters with the experiments. The refractive indexes used in the simulation for the glass substrate and the  $\text{Al}_2\text{O}_3$  layer were 1.5 and 1.62, respectively. An experimentally obtained optical constant for silver<sup>35</sup> was used in all the simulations in this paper. A Gaussian beam of 633 nm wavelength was used to generate SPPs in the nano-wires. Transitions in the symmetry of the SPP field were clearly observed in the simulations (Fig. 2). Before the wave arrives at the locations with broken symmetry, the field shows a symmetric profile (the small asymmetry is due to the reflection of SPPs). After passing the symmetry-broken location, the plasmon wave propagates in a zigzag route which results from the coherent superposition of two guiding modes with different symmetries. The field patterns agree

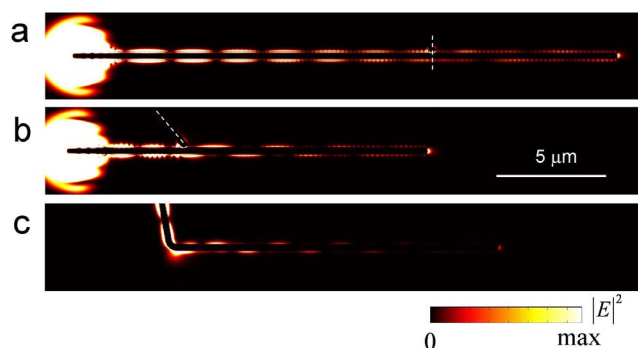


**Figure 2 | Simulation results of field intensity distributions for the mode conversions in the three kinds of experimental structures.** (a) Particle-NW structure, (b) branched NW and (c) bent NW. The distribution is on the horizontal section across the axis of the NWs. The radius of all the NWs and the particle is 150 nm. In both (a) and (b) the two component structures are separated by 1 nm.



well with the experimental results, indicating the mode conversion process in the symmetry-broken NW structures.

## Discussion

Eigenmodes of NW in uniform environment are analytical<sup>17,24,36</sup>, with the angular distributions as  $\sin m\phi$  or  $\cos m\phi$  ( $\phi$  is the angular coordinate in a cylindrical system). Figures 3(a) and 3(b) show the electric field distributions of the two lowest order modes in NW [sketch depicted in inset of Fig. 3(c)] calculated by finite element method (FEM). The lowest order  $TM_0$  mode is axially symmetric, and along any plane across the center of the wire the electric field of the  $TM_0$  mode is mirror-symmetric. The following  $m = 1$  order  $HE_1$  modes are doubly degenerate, with a  $90^\circ$  angle between polarizations<sup>24</sup>. Taking the mode polarized along the  $x$  direction as an example, the electric field is symmetric in the  $y$  direction, but anti-symmetric in the  $x$  direction. Figure 3(c) shows the dependence of the effective refractive index  $n_{\text{eff}}$  and the propagation length  $L_{\text{spp}}$  of  $TM_0$  and  $HE_1$  mode on the NW radius. The propagation length here is defined as the distance for the SPP intensity to decay to  $1/e$  of the original intensity. The NWs with considerable mode confinement and propagation length for practical use are multimode waveguides. Generally, the SPPs propagating on the NW are the superposition of  $TM_0$  and  $HE_1$  modes. For the two modes with initial phase as shown in Figs. 3(a) and 3(b), their interference leads to asymmetric field distribution in the  $x$  direction, with most fields distributed on the right side of the NW. Along the propagation direction, the two modes will accumulate different phase changes. When the phase difference reaches  $\pi$ , the maxima of the field shift to the other side of the wire. The repetitions of the shifting of the field maximum along the NW lead to the zigzag propagation route with the period  $L_p$  given by  $L_p = \lambda/(n_0 - n_1)$ , where  $n_0$  and  $n_1$  is the effective refractive index of the  $TM_0$  and the  $HE_1$  modes, respectively.

The symmetry of the eigenmodes is related to the symmetry of the waveguide structure. For a NW deposited on a substrate as the configuration in experiments and simulations above, the structure is more complex but also has mirror-symmetry in the direction parallel to the interface of the substrate (horizontal direction). The field distribution of the eigenmodes will also be mirror-symmetric or antisymmetric in the horizontal direction, verified by the four lowest order eigenmodes ( $H_0$ ,  $H_1$ ,  $H_2$  and  $H_3$ ) shown in Fig. S3 in supplementary information. For the laser light with polarization parallel to the nanowire, only the mirror-symmetric fundamental mode  $H_0$  and the third-order mode  $H_2$  can be generated directly. Their superposition leads to the periodic distributions before the wave arrives at locations with broken symmetry in Figs. 1(b)–(d)<sup>21</sup>. After these symmetry-broken locations, the two generated modes partly convert to mirror-antisymmetric  $H_1$  mode (and a small amount of  $H_3$  mode). The superposition of  $H_0$  and  $H_1$  modes leads to the zigzag route of SPP propagation observed in experiments and simulations above. The zigzag routes for SPPs on structures in uniform environment and on substrate have similar underlying physics. As discussed below, they also share the same mode-conversion mechanism. As shown by Fig. S4 in supplementary information, for single  $TM_0$  mode as input, the mode conversions also happen for the three similar structures in uniform environment. Hereafter, we discuss the mechanism of the mode conversion based on the structure in uniform environment, which can also be applied to the structure on substrate. In NWs suitable for waveguiding, the modes with higher order than  $HE_1$  mode are cut off. Therefore, we mainly discuss the conversion between the  $TM_0$  mode and  $HE_1$  mode. The mechanism can be generalized to conversions between more guiding modes.

The occurrence of mode conversions in the NWs with structural symmetry breaking can be directly understood by considering the symmetry of the modes in NW discussed above. In a single ideal NW, different modes are orthogonal and there is no cross-talk. However, when the structural symmetry is broken locally, the orthogonality

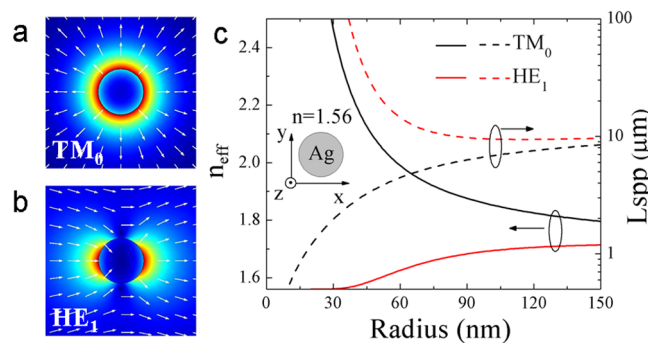


**Figure 3 | Two lowest order modes supported in silver NW.** (a–b) Electric field distribution of  $TM_0$  (a) and  $HE_1$  (b) modes in a silver NW with a radius of 60 nm at the wavelength  $\lambda = 633$  nm for vacuum. The two modes have different symmetry. (c) The effective refractive index and propagation length of the  $TM_0$  and  $HE_1$  modes as a function of the NW radius.

fails and the conversion between modes occurs. Here, the particle-NW structure in uniform dielectric environment is taken as an example for the interpretation, as shown in Fig. 4(a). We consider a wave of  $TM_0$  mode  $E_0(\mathbf{R})$  [Fig. 3(a)] propagating along the silver NW with its original wave front  $T_{in}(\mathbf{R})$ , shown in Fig. 4(a). Here  $\mathbf{R}$  is the position vector in the plane perpendicular to the NW. The structure has mirror symmetry in the  $y$  direction, but in the  $x$  direction the symmetry is broken. The output wave front  $T_{out}(\mathbf{R})$  will preserve the symmetry in the  $y$  direction, while the symmetry in the  $x$  direction will be disturbed. The  $T_{out}(\mathbf{R})$  with changed symmetry will have a nonzero expansion coefficient for  $HE_1$  mode:  $\int T_{out}(\mathbf{R})E_1(\mathbf{R})d\mathbf{R} \neq 0$ , where  $E_1(\mathbf{R})$  is the field distribution of  $HE_1$  mode [Fig. 3(b)]. Therefore, the structural symmetry breaking induces nonzero component of  $HE_1$  mode in the output, which implies a mode conversion process. The above analyses are also applicable for the mode conversions in branched NW and bent NW, as well as the mode conversions in structures on substrate. Using similar analysis for structures on the substrate, we can infer that both the  $H_0$  mode and  $H_2$  mode contribute to the conversion to the  $H_1$  mode (Fig. S3 in supplementary information).

Because of the reciprocity, in the same structure the backward conversion from  $HE_1$  mode to  $TM_0$  mode can also happen (from  $H_1$  mode to  $H_0$  mode for structure on the substrate, see Fig. S2 in supplementary information) with equal conversion efficiency. In a more general situation, when taking a superposition of the  $TM_0$  and  $HE_1$  as input, the  $T_{in}(\mathbf{R})$  can be expressed as  $[C_0, C_1]^T$ , where  $C_0$  and  $C_1$  are the expansion coefficients of  $T_{in}(\mathbf{R})$  by the  $TM_0$  and  $HE_1$  modes, normalized by  $|C_0|^2 + |C_1|^2 = 1$ . Similarly, the output can be expressed as  $[C'_0, C'_1]^T$ . The structure can be taken as a symmetric 4-port lossy network, similar to that in electronic and microwave engineering, for which the conversion process can be described by using the S-parameter<sup>37</sup> as:

$$S \cdot [C_0, C_1]^T = [C'_0, C'_1]^T \quad (1)$$

where  $S$  is a  $2 \times 2$  diagonal matrix, with its elements as  $S_{ij}$  ( $i, j = 0, 1$ ). The conversion efficiency from  $i$  mode to  $j$  mode ( $i, j = 0, 1$  correspond to the  $TM_0$  and  $HE_1$  modes) can be expressed as:  $\eta_{ij} = |S_{ij}|^2$ .

We further interpret the underlying physics of the mode-conversion phenomena. The mode conversion in bent NWs is analogous to the mode conversion in ordinary dielectric circular waveguides and can be interpreted by the coupled mode theory<sup>38</sup>. Mode conversions by introducing a new structure near the NW have good tunability and similar origin. The particle-NW structure is selected for a careful treatment to reveal the mode conversion mechanism. From an intu-

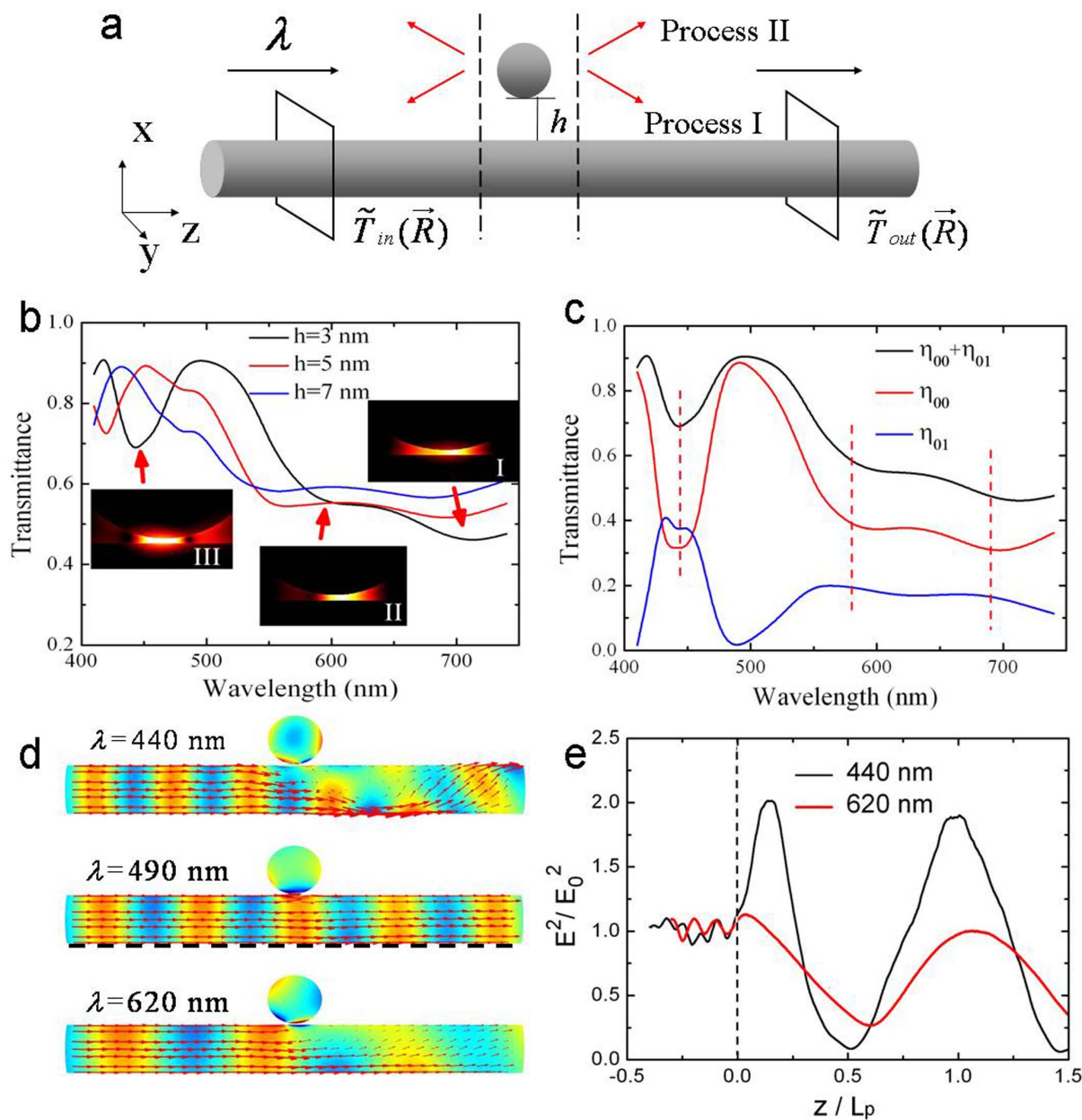


**Figure 4 | Mechanism of the mode conversion in the particle-NW structure.** (a) Schematic illustration of the particle induced symmetry breaking of the structure for mode conversion in a silver NW. (b) Total transmittance spectra in particle-NW structures of different separation  $h$ . Insets show the electric field distributions ( $|E|$ ) of the resonant gap modes corresponding to the drops in the spectrum for  $h = 3$  nm. (c) Mode conversion efficiency and transmittance for different wavelengths, with a constant separation  $h = 3$  nm. Blue: efficiency of mode conversion from  $TM_0$  mode to  $HE_1$  mode. Red: the transmittance spectra of the remaining  $TM_0$  mode. Black: the total transmittance spectrum. The dashed lines mark the approximate positions of the three resonance modes. (d) Distributions of power flow (arrows) and instant surface charge (color coordinate) for  $\lambda = 440$  nm (on resonance and Process I dominant),  $\lambda = 490$  nm (off resonance and Process I dominant) and  $620$  nm (off resonance and Process II dominant). (e) Distribution of electric field intensity (normalized by the incident field intensity  $E_0^2$ ) at the bottom of the NW [marked by black dashed line in middle panel of (d)]. The position is normalized by the period  $L_p$  with the origin set at the center of the particle.

itive point of view, the mode conversion process in the particle-NW structure is actually a scattering process. The scattering at the particle can be decomposed into two processes, as denoted in Fig. 4(a). In the process I, the scattering of power is coupled back into the NW, while the process II corresponds to the direct scattering of power into free space. Both the two scattering processes contribute to the mode conversion, as discussed below.

More careful simulation analyses are used to give quantitative descriptions of the mode conversions. The uniform environment has a refractive index of 1.56. The material loss of the NW is ignored here by eliminating the imaginary part of the permittivity of silver in

the simulation. The material loss of the NW mainly reduces the total transmittance due to the attenuations of the SPP propagation, but has little effect on the scattering near the nanoparticle. It will not violate the conversion mechanism we discussed below. In Fig. 4(b), the transmittance spectra for different separations  $h$  between the nanoparticle and NW are shown. The drops in the spectra correspond to the resonant modes localized in the nanogap between the NW and the particle, as shown by the insets, with the order defined by the number of antinodes in their field distributions. At resonances, larger power is scattered into the free space, which results in higher losses and the drops in the spectra. All the resonant modes

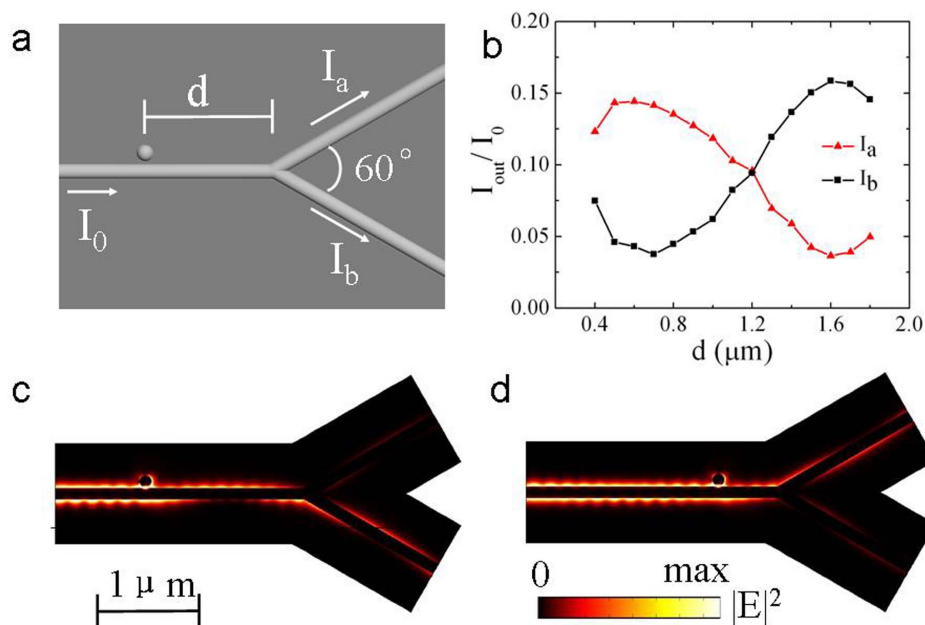


**Figure 5 | Application of nanoparticle-mediated mode conversion for a tunable switch in a branched NW.** (a) The sketch of the proposed switch structure. (b) The output intensities  $I_{out}$  at the two branches, normalized by the input intensity  $I_0$  as a function of particle locations. (c–d) Electric field distributions for the two states of power switched between the two output branches. The radiuses of the NW and the particle are both 60 nm and their separation is 5 nm.

are highly localized, which create hotspots of electromagnetic field and are responsible for the enhanced Raman scattering in particle-NW structure<sup>39,40</sup>. As the separation between particle and NW decreases, the resonant modes red-shift, similar to the behavior of localized modes for coupled nanoparticles<sup>2</sup>. Figure 4(c) shows the conversion efficiency from  $TM_0$  mode to  $HE_1$  mode  $\eta_{01}$  and the transmission efficiency for the remaining  $TM_0$  mode  $\eta_{00}$  for  $h = 3$  nm (see Fig. S5 in supplementary information for the dependence of mode conversion on the separation  $h$ ). For clarity, the total transmittance spectrum is also plotted in Fig. 4(c). As can be seen, although the scattering loss is larger at the resonant wavelengths, the conversion efficiency  $\eta_{01}$  reaches the maxima at the resonances, shown as peaks in the blue curve.

The physical picture of the conversion process is revealed by the distribution of time-averaged power flow at both resonance and off-resonance wavelengths shown in Fig. 4(d). The power flows uniformly through the NW before the particle. When the light arrives at the particle, the resonant gap mode between the particle and the NW is excited for  $\lambda = 440$  nm. The highly localized field in the gap can act as a point source to couple power back into the NW with a new component of  $HE_1$  mode. The point source can excite the SPPs in NWs in a high efficiency, so the scattering of the gap mode includes remarkable process I described in Fig. 4(a). As can be seen in Fig. 4(d), the power flow is directed away from the nanoparticle to the bottom of the NW. Here the wave front becomes asymmetric, which implies a new  $HE_1$  mode comes into being. Due to the scattering, the field intensity at the bottom of the NW at the right side of the particle, i.e.,  $z > 0$  ( $z$  is set 0 at the center of the nanoparticle) is doubled as shown by black curve in Fig. 4(e). The scattering reaches the maximum at the resonance wavelength, giving a higher conversion efficiency  $\eta_{01}$ . When the gap is off-resonant at 490 nm wavelength, the field propagating on the NW is less scattered and the wave front is hardly disturbed as shown in the middle panel in Fig. 4(d), resulting in a much lower conversion efficiency.

For longer wavelength of 620 nm, although the gap is off-resonant, the conversion efficiency is still not low. The  $TM_0$  mode for longer wavelength has a wider field distribution with more overlap with the nanoparticle, leading to larger scattering on the particle as

shown by the visible scattering light near the particle in Fig. 1(b). However, in this scattering process, the scattering field on the particle is not highly localized as the gap modes, so that it can not efficiently excite the SPP mode in the NW. This scattering mainly radiates into the free space and leads to higher scattering loss, which agrees with the lower transmission intensity of  $\eta_{00} + \eta_{01}$  for 620 nm in Fig. 4(c) and corresponds to the process II in Fig. 4(a). As shown in the bottom panel in Fig. 4(d), for  $\lambda = 620$  nm the power flow on the top side of the NW near the particle is scattered without flowing to the bottom side, and the power flow at the bottom maintains its original distribution. The field distribution on the wave front for  $z > 0$  becomes asymmetric, which means this scattering also induce a new component of  $HE_1$  mode. The red curve in Fig. 4(e) shows that the field on the NW bottom at the right side near the particle is equal to the incident intensity. After the particle, the remaining SPP power begins to spread up to the top side of the NW and finally forms the zigzag shape. The mechanism discussed above can also be applied to the mode conversion in branched NW structure, as shown by Fig. S6 in the supplementary information.

The mode conversion by the nanoparticle can be applied to control flexibly the propagation behavior of SPPs. An example is schematically shown in Fig. 5(a) for a structure composed of a branched NW and a nearby nanoparticle. In the simulation, the  $TM_0$  mode is taken as input and material loss of silver is considered. By tuning the position of the nanoparticle, power is switched between the two NW branches, realizing the function of a single-pole double-throw switch, as shown in Fig 5(b). This function is achieved owing to the tunable zigzag propagating route, depicted in Figs. 5(c) and 5(d). With the shift of the particle, the maximum of the electric field moves from one side to the other side of the NW, realizing the power switching between the two output branches. Apart from the nanoparticle, other structures introduced to break the local symmetry near the NW can also mediate the mode conversion, following similar principles. In plasmonic NW networks, the mode conversion at the junctions can strongly influence the propagation of SPPs. Therefore, by designing the structure parameters and tailoring the mode conversion processes, good-performance nanophotonic devices can be rationally achieved.



The symmetry breaking, that is responsible for the mode conversion in the silver NW, can also be achieved in other forms. For example, the inhomogeneity of the refractive index of environment around the NW also introduces a kind of symmetry breaking and leads to the mode conversion. In this situation, the fast-speed control to the mode conversion can be achieved by using active materials, for example the electro-optic materials, which can be used for electrically controlled nanophotonic devices. It should be noted that the bent NW and branched NW are the fundamental structures for constructing NW networks. The mode conversion is an ever-present effect in the NW network, and is decisive for the signal transmission, which has already been manifested in the NW-based logical gates<sup>22,23</sup>. Therefore, the mode conversion is a crucial effect which should be considered carefully for designing NW-based nanophotonic devices and circuits.

In conclusion, we have shown experimentally and theoretically that mode conversion can occur in plasmonic NWs with local structural symmetry breaking. By analyzing the symmetry of the modes supported in the NW, we find the conversion originates from the symmetry change of wave front induced by the structural symmetry breaking. Careful simulations are used to analyze the conversion processes in nanoparticle-NW structure and reveal that the conversion is a result of the scattering of localized modes in the nanogap and on the nanoparticle. This mode conversion phenomenon is important for designing new plasmonic NW based optical circuits and devices, and can be applied to flexibly control the propagation behavior of plasmons at nanoscale.

## Methods

**Sample and measurements.** The Ag NWs and nanoparticles were synthesized by a wet chemical method and dispersed in ethanol. They were dropped on a cleaned glass substrate. Then an Al<sub>2</sub>O<sub>3</sub> layer of 30 nm or 50 nm thickness was deposited using atomic layer deposition. Finally, semiconductor QDs with emission wavelength centered at 655 nm were spin-coated onto the sample surface.

Optical measurements were performed on an upright optical microscope. Laser light of 633 nm was focused onto the end of the NW through a  $\times 100$  (NA 0.95) objective. The image was collected by the same objective and directed to a CCD camera. To record the QD fluorescence, a long-pass edge filter was used to block the laser light.

**Simulation method.** The full-wave simulation of the experimental structures was performed using the commercial software Lumerical Solution. The FDTD method is chosen here to model the large system with substrate. Mesh size of 5 nm and boundary of perfectly matched layers (PML) are found accurate enough for the simulation. All the structure parameters are chosen according to the experiment sample.

All simulations for the eigenmodes and the field in the structures immersed in uniform dielectric environment are based on finite element method (FEM), using commercial software package COMSOL. The field distributions of the eigenmodes in NWs were directly obtained by mode analyses. Due to the difficulty of the FEM carrying out large scale full-wave simulations, we adopted structures formed by thinner and shorter NWs. To simulate the mode-conversion process, single TM<sub>0</sub> mode was used as input for the NWs to solve the field distributions. The single mode input is realized by the so-called port boundary condition. The port boundary conditions are also used at the output to directly absorb the different modes on the NW at the output. At the same time, the boundary condition can provide the mode components it absorbed at the output, because the software automatically calculates expansion coefficients of the different modes using the output field profile. Then the transmittance for the different modes in Fig. 4 can be derived.

- Xu, H. X., Bjerneld, E. J., Käll, M. & Börjesson, L. Spectroscopy of single hemoglobin molecules by surface enhanced Raman scattering. *Phys. Rev. Lett.* **83**, 4357–4360 (1999).
- Xu, H. X., Aizpurua, J., Käll, M. & Apell, P. Electromagnetic contributions to single-molecule sensitivity in surface-enhanced Raman scattering. *Phys. Rev. E* **62**, 4318–4324 (2000).
- Mühlschlegel, P., Eisler, H.-J., Martin, O. J. F., Hecht, B. & Pohl, D. W. Resonant optical antennas. *Science* **308**, 1607–1609 (2005).
- Kim, S. *et al.* High-harmonic generation by resonant plasmon field enhancement. *Nature* **453**, 757–760 (2008).
- Fang, N., Lee, H., Sun, C. & Zhang, X. Sub-diffraction-limited optical imaging with a silver superlens. *Science* **308**, 534–537 (2005).
- Kawata, S., Inoué, Y. & Verma, P. Plasmonics for near-field nano-imaging and superlensing. *Nat. Photon.* **3**, 388–394 (2009).
- Bozhevolnyi, S. I., Volkov, V. S., Devaux, E., Laluet, J. Y. & Ebbesen, T. W. Channel plasmon subwavelength waveguide components including interferometers and ring resonators. *Nature* **440**, 508–511 (2006).
- Ebbesen, T. W., Genet, C. & Bozhevolnyi, S. I. Surface-plasmon circuitry. *Phys. Today* **61**, 44–50 (2008).
- Gramotnev, D. K. & Bozhevolnyi, S. I. Plasmonics beyond the diffraction limit. *Nat. Photon.* **4**, 83–91 (2010).
- Sanders, A. W. *et al.* Observation of plasmon propagation, redirection, and fan-out in silver nanowires. *Nano Lett.* **6**, 1822–1826 (2006).
- Guo, X. *et al.* Direct coupling of plasmonic and photonic nanowires for hybrid nanophotonic components and circuits. *Nano Lett.* **9**, 4515–4519 (2009).
- Ditlbacher, H. *et al.* Silver nanowires as surface plasmon resonators. *Phys. Rev. Lett.* **95**, 257403 (2005).
- Allione, M., Temnov, V. V., Fedutik, Y., Woggon, U. & Artemyev, M. V. Surface plasmon mediated interference phenomena in low-Q silver nanowire cavities. *Nano Lett.* **8**, 31–35 (2008).
- Li, Z. P. *et al.* Directional light emission from propagating surface plasmons of silver nanowires. *Nano Lett.* **9**, 4383–4386 (2009).
- Shegai, T. *et al.* Unidirectional broadband light emission from supported plasmonic nanowires. *Nano Lett.* **11**, 706–711 (2011).
- Chang, D. E., Sørensen, A. S., Hemmer, P. R. & Lukin, M. D. Quantum optics with surface plasmons. *Phys. Rev. Lett.* **97**, 053002 (2006).
- Chang, D. E., Sørensen, A. S., Hemmer, P. R. & Lukin, M. D. Strong coupling of single emitters to surface plasmons. *Phys. Rev. B* **76**, 035420 (2007).
- Akimov, A. V. *et al.* Generation of single optical plasmons in metallic nanowires coupled to quantum dots. *Nature* **450**, 402–406 (2007).
- Wei, H., Ratchford, D., Li, X. Q., Xu, H. X. & Shih, C.-K. Propagating surface plasmon induced photon emission from quantum dots. *Nano Lett.* **9**, 4168–4171 (2009).
- Fang, Y. R. *et al.* Branched silver nanowires as controllable plasmon routers. *Nano Lett.* **10**, 1950–1954 (2010).
- Wei, H., Zhang, S. P., Tian, X. R. & Xu, H. X. Highly tunable propagating surface plasmons on supported silver nanowires. *Proc. Natl. Acad. Sci. USA* **110**, 4494–4499 (2013).
- Wei, H. *et al.* Quantum dot-based local field imaging reveals plasmon-based interferometric logic in silver nanowire networks. *Nano Lett.* **11**, 471–475 (2011).
- Wei, H., Wang, Z. X., Tian, X. R., Käll, M. & Xu, H. X. Cascaded logic gates in nanophotonic plasmon networks. *Nat. Commun.* **2**, 387 (2011).
- Zhang, S. P. *et al.* Chiral surface plasmon polaritons on metallic nanowires. *Phys. Rev. Lett.* **107**, 096801 (2011).
- Wang, H. *et al.* Symmetry breaking in individual plasmonic nanoparticles. *Proc. Natl. Acad. Sci. USA* **103**, 10856–10860 (2006).
- Wu, Y. P. & Nordlander, P. Plasmon hybridization in nanoshells with a nonconcentric core. *J. Chem. Phys.* **125**, 124708 (2006).
- Luk'yanchuk, B. *et al.* The Fano resonance in plasmonic nanostructures and metamaterials. *Nat. Mater.* **9**, 707–715 (2010).
- Hao, F. *et al.* Symmetry breaking in plasmonic nanocavities: subradiant LSPR sensing and a tunable Fano resonance. *Nano Lett.* **8**, 3983–3988 (2008).
- Zhang, S., Genov, D. A., Wang, Y., Liu, M. & Zhang, X. Plasmon-induced transparency in metamaterials. *Phys. Rev. Lett.* **101**, 047401 (2008).
- Liu, N. *et al.* Plasmonic analogue of electromagnetically induced transparency at the Drude damping limit. *Nat. Mater.* **8**, 758–762 (2009).
- Zhang, Z. *et al.* Manipulating nanoscale light fields with the asymmetric bowtie nano-colorsorter. *Nano Lett.* **9**, 4505–4509 (2009).
- Shegai, T. *et al.* A bimetallic nanoantenna for directional colour routing. *Nat. Commun.* **2**, 481 (2011).
- Pendry, J. B., Holden, A. J., Robbins, D. J. & Stewart, W. J. Magnetism from conductors and enhanced nonlinear phenomena. *IEEE Trans. Microwave Theory Tech.* **47**, 2075–2084 (1999).
- Liu, N., Liu, H., Zhu, S. N. & Giessen, H. Stereometamaterials. *Nat. Photon.* **3**, 157–162 (2009).
- Johnson, P. B. & Christy, R. W. Optical constants of the noble metals. *Phys. Rev. B* **6**, 4370–4379 (1972).
- Jackson, J. D. *Classical Electrodynamics*. (Wiley; New York, 1999).
- Pozar, M. D. *Microwave Engineering*. (Wiley, New York, 1998).
- Marcuse, D. *Theory of Dielectric Optical Waveguides*. (Academic Press, San Diego, 1991).
- Wei, H. *et al.* Polarization dependence of surface-enhanced Raman scattering in gold nanoparticle-nanowire systems. *Nano Lett.* **8**, 2497–2502 (2008).
- Fang, Y. R., Wei, H., Hao, F., Nordlander, P. & Xu, H. X. Remote-excitation surface-enhanced Raman scattering using propagating Ag nanowire plasmons. *Nano Lett.* **9**, 2049–2053 (2009).

## Acknowledgments

This work was supported by National Natural Science Foundation of China (Grant Nos. 11134013, 11227407, 11374012 and 61210017), The Ministry of Science and Technology of China (Grant No. 2012YQ12006005), “Knowledge Innovation Project” (Grant No. KJCX2-EW-W04) and Youth Innovation Promotion Association of Chinese Academy of Sciences (CAS). The authors thank the Laboratory of Microfabrication in the Institute of Physics, CAS for experimental support.



## Author contributions

H.X.X. supervised the project. D.P. and H.W. developed the concept. H.W. and Z.L.J. performed the experiments. D.P. performed the simulations and gave the explanation. D.P., H.W. and H.X.X. wrote the manuscript.

## Additional information

**Supplementary information** accompanies this paper at <http://www.nature.com/scientificreports>

**Competing financial interests:** The authors declare no competing financial interests.

**How to cite this article:** Pan, D., Wei, H., Jia, Z.L. & Xu, H.X. Mode Conversion of Propagating Surface Plasmons in Nanophotonic Networks Induced by Structural Symmetry Breaking. *Sci. Rep.* **4**, 4993; DOI:10.1038/srep04993 (2014).



This work is licensed under a Creative Commons Attribution-NonCommercial-NoDerivs 3.0 Unported License. The images in this article are included in the article's Creative Commons license, unless indicated otherwise in the image credit; if the image is not included under the Creative Commons license, users will need to obtain permission from the license holder in order to reproduce the image. To view a copy of this license, visit <http://creativecommons.org/licenses/by-nc-nd/3.0/>